FISEVIER

Contents lists available at ScienceDirect

# Journal of Materials Research and Technology

journal homepage: www.elsevier.com/locate/jmrt





# Comprehensive analysis of thermophysical properties of the $NaNO_3$ – $KNO_3$ mixture with metastable phases

D. Sergeev<sup>a,c,\*</sup>, G. Nénert<sup>b</sup>, D. Rapp<sup>a</sup>, F. Beckstein<sup>a</sup>, M. Schöneich<sup>a</sup>, M. Müller<sup>c</sup>, J. Gertenbach<sup>b</sup>

- <sup>a</sup> NETZSCH-Gerätebau GmbH, Selb, D-95100, Germany
- <sup>b</sup> Malvern Panalytical B.V., Almelo, 7602 EA, the Netherlands
- <sup>c</sup> Forschungszentrum Jülich GmbH, IMD-1, Jülich, D-52425, Germany

# ARTICLE INFO

Keywords: Salt systems Metastable phases Thermal analysis X-ray diffraction

#### ABSTRACT

This study focuses on the comprehensive analysis of the  $NaNO_3$ –KNO $_3$  system, a salt mixture that is extensively used as a heat transfer fluid and thermal energy storage material in concentrated solar power (CSP) plants. Despite its common application, discrepancies exist in the reported equilibrium phase diagrams, largely due to the formation of metastable phases influenced by experimental conditions. This work combines various thermophysical methods, including differential scanning calorimetry, thermomechanical analysis, laser flash analysis, and high-temperature X-ray diffraction, to resolve these discrepancies. The thermal and structural properties of a 50 mol %  $NaNO_3$  – 50 mol %  $NaNO_3$  mixture have been determined. Significant differences in phase transition temperatures and volume were observed between the first and second heating cycles. In-situ HTXRD confirmed the formation of metastable solid solution phases upon cooling to room temperature after the first heating. The comprehensive analysis provided insights into the equilibrium and metastable states of the mixture, highlighting the importance of combining thermal analysis techniques with XRD for a thorough characterization of material properties.

# 1. Introduction

During the last century, a large amount of experimental and computational data for different kind of salt systems has been collected and is currently represented in the relevant thermodynamic databases. The main interest to these systems is related to the use as heat transfer fluids or chemical reactants in key industries such as metallurgy, nuclear and solar energy, because they have unique thermophysical properties, coupled with their relatively low costs. The combination of salts with different cations and anions greatly increases the variety of applications. For example the NaNO<sub>3</sub>–KNO<sub>3</sub> system has been extensively studied due to its applications as heat transfer fluid and thermal energy storage (TES) material for concentrated solar power (CSP) plants. Currently, in most CSP plants so-called SolarSalt (mixture of 60 wt% NaNO<sub>3</sub> and 40 wt% KNO<sub>3</sub>) is used due to its favorable thermophysical properties. However, its operational temperature is constrained to 560–565 °C due to thermal stability limitations [1–6].

Despite numerous studies on this system [1-21], significant

inconsistencies still exist in the reported phase diagrams. These inconsistencies are particularly evident in the equilibrium phase relations, which are crucial for thermodynamic modelling and reliable computational predictions of multicomponent systems. These predictions are essential for identifying optimal salt compositions while reducing dependence on trial-and-error experimental methods. Achieving accurate calculations for binary and multicomponent systems requires a precise and comprehensive description of the Gibbs energies of both solid and liquid phases. This approach becomes even more complex in the presence of solid solutions, particularly when the formation of metastable phases during experiments leads to misinterpretations of phase equilibria.

Thermodynamic software uses typically two main types of the phase diagram [11], e.g. in the FactSage [12] - FTsalt and FTfrtz databases (Figs. 1 and 2), which are based on thermodynamic evaluations of previous experimental data for this system [13–17]. Fig. 1 (FTsalt) representing the first type of the phase diagram, which considers the solid-liquid equilibrium as the eutectic type [13,14,17–19] with the

<sup>\*</sup> Corresponding author. NETZSCH-Gerätebau GmbH, Selb, D-95100, Germany. *E-mail addresses*: dmitry.sergeev@netzsch.com, d.sergeev@fz-juelich.de (D. Sergeev).

melting of two phases (limited solid solutions based on the high temperatures modifications of NaNO $_3$  and KNO $_3$ ). Fig. 2 representing the phase diagram from FTfrtz database features a loop with a minimum (azeotrope type) and a continuous solid solution (K1, Fig. 2) between the high-temperature forms of NaNO $_3$  and KNO $_3$  [11,20,21]. One of the reasons for these discrepancies is the formation of metastable phases during experimental study of the salt mixtures, which can depend on many different parameters of the experimental devices (differential thermal analysis (DTA), differential scanning calorimetry (DSC), thermomechanical analysis (TMA), laser/light flash analysis (LFA) and XRD), e.g. on sample preparation procedure as well as on the temperature program. Similar kinetic effects are observed also for other salt systems, e.g. for the binary KNO $_3$  – Ca(NO $_3$ ) $_2$  [22] and the reciprocal K, Ca//Cl, NO $_3$  system [23].

In order to develop a consistent and reliable thermodynamic database that can accurately predict phase equilibria in multicomponent molten salt systems, it is essential to perform a comprehensive analysis that takes into account the formation of metastable phases. In particular, a combination of thermal analysis techniques with high temperature insitu X-ray diffraction is crucial to resolve structural ambiguities in these systems and improve the accuracy of thermodynamic modelling.

In this study, we present a detailed investigation of the NaNO $_3$ –KNO $_3$  system by combining DSC, TMA, and LFA with in-situ X-ray powder diffraction. This integrated approach enables a deeper understanding of the phase diagram and the thermal behaviour of this system, specifically focusing on the 50 mol % NaNO $_3$  – 50 mol % KNO $_3$  composition, which was selected as a representative composition for the study of thermophysical properties of this system. A newly designed container for thermomechanical analysis (TMA) is employed for the first time to precisely determine the volume change of both the solid and liquid phases. In-situ TMA observations of the sintering process are important for minimizing errors in the determination of thermal diffusivity obtained from LFA results. The comprehensive analysis conducted in this work allows for the precise identification of metastable phase formation during heating and cooling cycles and facilitates a more accurate interpretation of experimental results obtained through different

techniques.

#### 2. Materials and methods

To clarify the discrepancies of literature data, a comprehensive analysis involving different of thermal analysis and X-ray diffraction techniques has been used to study the 50 mol % NaNO<sub>3</sub> - 50 mol % KNO<sub>3</sub> mixture. This salt mixture was synthesized by blending high-purity NaNO<sub>3</sub> (99.995 %) and KNO<sub>3</sub> (99.999 %) acquired from Sigma-Aldrich. The pure compounds were mixed according to the mass ratio in a glazed porcelain crucible and heated to 300 °C under an air atmosphere. Afterwards, the prepared mixture was grinded and stored in an exicator. Thermogravimetric analysis of the resulting mixture revealed minimal mass loss (0.06 %) upon heating the sample to 400 °C over two cycles, indicating a low content of absorbed water (Fig. 1s in supplementary material). The ratio and purity of the initial composition was confirmed by the XRD results. This study is focused mainly on the formation of metastable phases in the solid phase. Therefore, just a limited temperature range up to 360 °C was applied for experiments in the liquid phase, which allowed us to avoid mass loss during these experiments. Traditionally salt materials tend to show a poor particle statistic, precluding accurate and reliable X-ray powder diffraction. To prevent this issue, the sample of 50 mol % KNO<sub>3</sub> – 50 mol % NaNO<sub>3</sub> was spun to improve particle statistics in a quartz capillary of  $\emptyset = 0.7$  mm. In-situ Xray powder diffraction experiments were determined using an Empyrean Series 3 diffractometer using a Cu X-ray tube, a focusing mirror, Soller slits of 0.04 rad, and a 1Der strip detector. The sample in the quartz capillary was heated using a non-ambient chamber mounted on the diffractometer. The various isoline plots and the Pawley fits were carried out using the HighScore suite [24].

NETZSCH DSC 204F1 Phoenix has been used for determination of heat capacity of the 50 mol % NaNO $_3$  - 50 mol % KNO $_3$  mixture. The experiments were performed in aluminum crucibles with pierced lid and a heating rate of 10 K/min and 40 ml/min flow rate of nitrogen. Three measurements (baseline, sapphire as a reference material and sample) under identical conditions were performed for determination of the heat

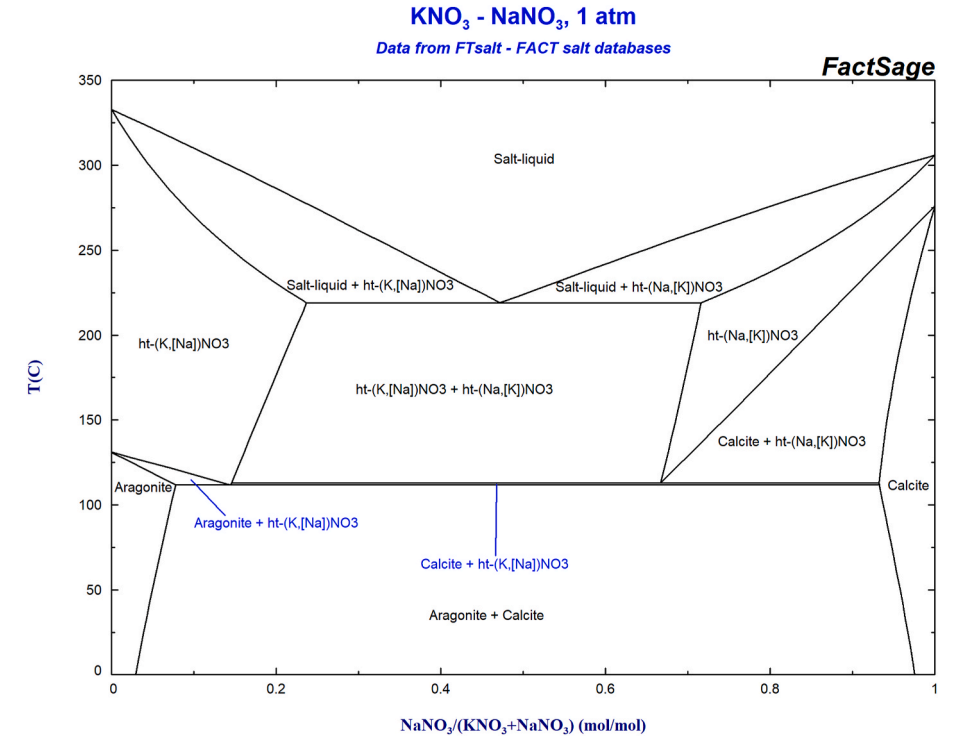


Fig. 1. Phase diagram of the NaNO<sub>3</sub> - KNO<sub>3</sub> system from FTsalt database in FactSage.

capacity according to the ratio method. Phase changes of the pure metals In, Sn, Bi and Zn were used for temperature calibration. The average temperature deviation was  $\pm 1~^{\circ}\text{C}$  and the uncertainty for heat capacity was estimated to be  $\pm 3~\%$ .

For determination of the thermal expansion of the prepared sample NETZSCH TMA 402F1 Hyperion® was applied. The measurements were performed in a new designed graphite container (Fig. 2s in supplementary material) with a heating rate of 2 K/min under helium atmosphere (40 ml/min) and constant applied force of 50 mN. The calibration correction with sapphire cylinder (diameter 5.97 mm, length 4.99 mm) as a reference material was performed before the sample measurements under the same conditions. The calibration correction considers the expansion of the entire measuring system, including the pushrod, the sample holder and the container. The samples for TMA measurements were prepared using the pressing technique. The salt powder was pressed with a force of 20 kN (24 h, sample 1) and 7 kN (10 min, sample 2) to a pellet with a cylindrical shape (diameter 6.01 mm) and with an initial length of 4.57 mm and 4.91 mm respectively. The prepared samples were placed into the graphite container and heated according to the temperature program. The temperature programme consists of three cycles. The first cycle involves heating to 210 °C at 2 K/ min, followed by a 24 h isothermal step and then cooling back to 20 °C. The second cycle follows the same heating and cooling steps but omits the isothermal hold, allowing the reproducibility of the signal to be assessed. The third cycle extends the heating to 305 °C, above the melting temperature (222 °C), to study the thermal expansion of the sample in the liquid phase.

The thermal diffusivity measurements were conducted using a NETZSCH LFA 467 HyperFlash on a pressed salt pellet (20 kN, 24 h) with a diameter of 12.58 mm and a thickness of 1.048 mm. The analysis was carried out over three heating cycles, with stepwise temperature increments of 25  $^{\circ}$ C, reaching a maximum temperature of 185  $^{\circ}$ C. At each temperature step, three measurements were performed and averaged for the final evaluation. To enhance the absorption and emission of radiation, the prepared salt pellet was coated with a thin graphite layer.

Since the measurements were conducted exclusively in the solid

state, the single-layer model was applied for signal evaluation. A Xenon flash lamp generated a 600 µs light pulse to heat the front surface of the sample. A liquid nitrogen-cooled InSb photocell was used to detect the temperature response on the rear surface of the sample within a detection area of 3.7 mm in diameter. The resulting signals were analysed using the standard model based on Cape-Lehman, which accounts for non-uniform front-surface illumination and rear-face detection, with pulse correction applied based on an exponential model. To account for variations in sample thickness due to thermal expansion, the thermal diffusivity values were corrected based on measured thickness changes using the TMA results. The accuracy of the method was validated using Pyroceram as a reference material, measured in a wide temperature range from 25  $^{\circ}\text{C}$  to 500  $^{\circ}\text{C}$  . The deviation from the reference values was found to be less than 2 %. The total uncertainty in the obtained thermal diffusivity values was estimated to be 4 %, considering both the statistical deviation of the signal and thickness variations during measurement.

Determining thermal diffusivity in the liquid phase requires a specialized sample container for LFA measurements, as discussed in previous studies [25–28]. These studies highlight the significant challenges associated with accurately measuring the thermal diffusivity of molten salts, primarily due to the creeping effect [25–27]. Therefore, measurements in the liquid phase using LFA were not considered in this study.

#### 3. Results and discussion

Fig. 3 shows the DSC curves for the first and the second heating and cooling of the 50 mol % NaNO $_3$  - 50 mol % KNO $_3$  mixture. Upon initial heating, the data shows a continuous solid-solid phase transition in the temperature range from 110 °C to 173 °C, and melting at 222 °C. This is consistent with the phase diagram from FTfrtz database (Fig. 2). The second heating curve shows an additional solid-solid transition at 98 °C, which is reproducible when the sample is treated with additional heating and cooling cycles. In contrast to the initial heating, the salt mixture displays a behavior in subsequent heating cycles that is better

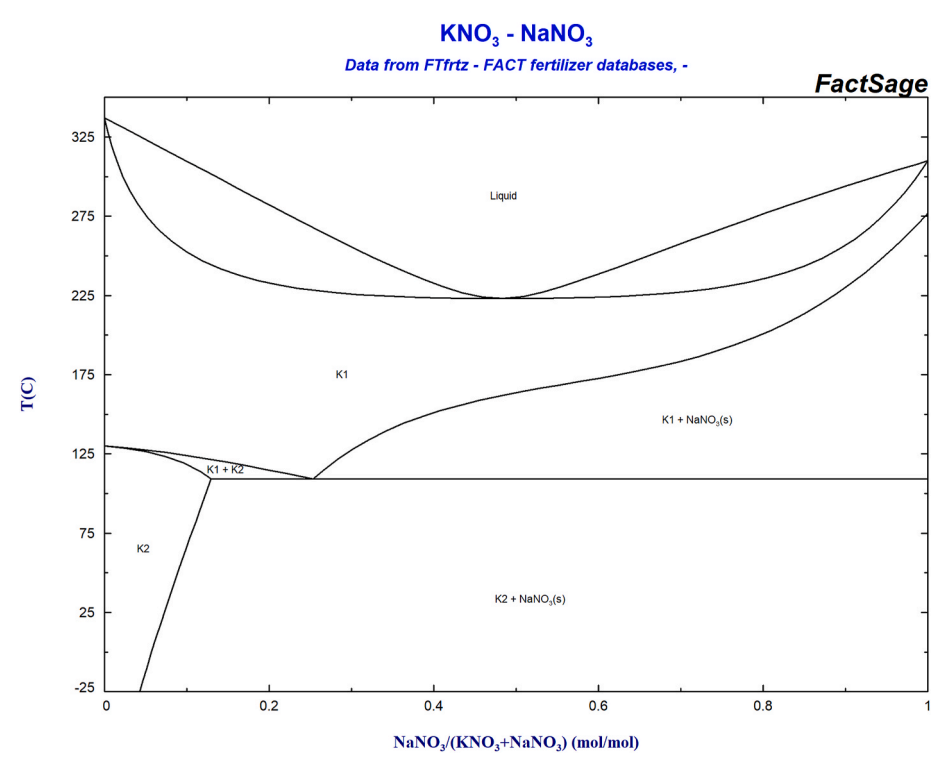


Fig. 2. Phase diagram of the NaNO<sub>3</sub> - KNO<sub>3</sub> system from FTfrtz database in FactSage.

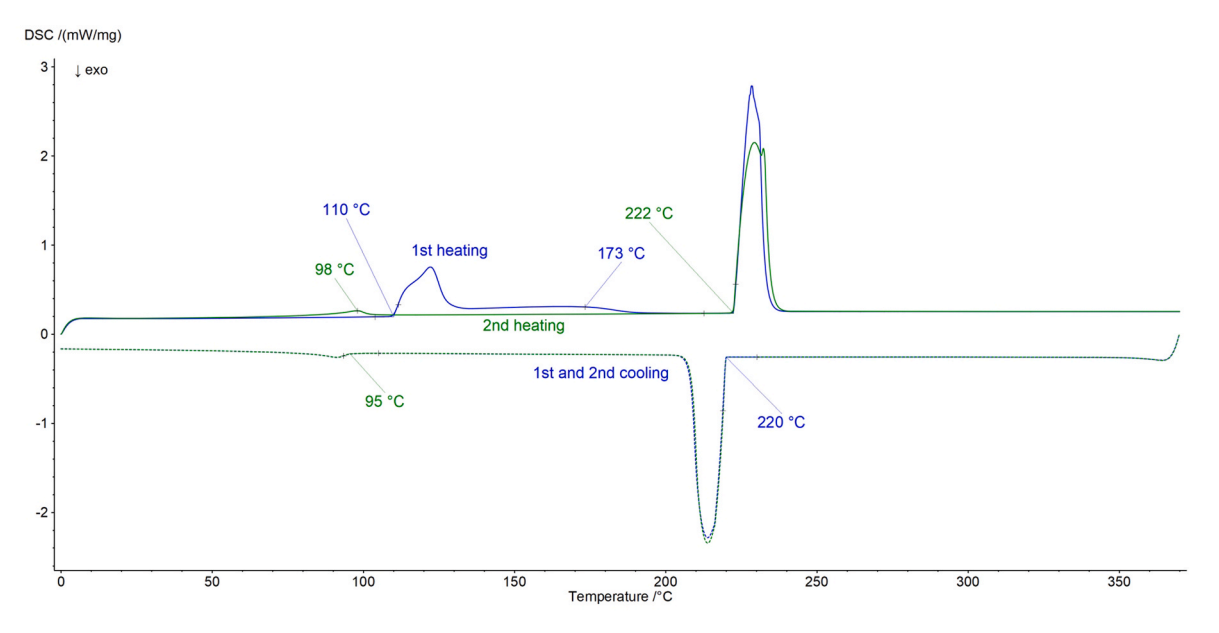


Fig. 3. DSC curves for the first and the second heating and cooling of the 50 mol % NaNO<sub>3</sub> - 50 mol % KNO<sub>3</sub> mixture.

described by the phase diagram from FTsalt database in FactSage (Fig. 1). After this set of experiments, the sample was allowed to equilibrate for 1 week at ambient temperature; it was not possible to reproduce the behavior of the first heating curve during the experiment. This would suggest that the second heating curve (Fig. 3) represents a metastable state of the 50 mol % NaNO $_3-50$  mol % KNO $_3$  mixture. Such effects should be considered by interpretation of phase diagrams that typically describe equilibrium conditions.

The apparent heat capacity and phase transition enthalpies were calculated from the DSC data based on the sensitivity calibration using a sapphire reference sample. The results of this evaluation are shown in Fig. 4. The comparison of the values obtained from the fusion enthalpy of the 50 mol % NaNO $_3$  – 50 mol % KNO $_3$  mixture shows a good

agreement with literature data of 101.6 J g $^{-1}$  [29] and 100.7 J g $^{-1}$  [30] within an uncertainty of 2 %. The specific heat capacity of the liquid phase remains almost constant in a wide temperature range from 240 °C to 360 °C, averaging 1.469 J g $^{-1}$  K $^{-1}$  and 1.488 J g $^{-1}$  K $^{-1}$  for the first-and the second heating cycles respectively. The average literature value of the 50 mol % NaNO3  $^-$  50 mol % KNO3 mixture is 1.492 J g $^{-1}$  K $^{-1}$  [27], which is in good agreement with the second heating values and corresponds within 2 % to the first heating values of specific heat capacity.

To confirm the DSC results, the same salt composition was tested using TMA and LFA devices. In this case the sample preparation procedure plays critical role in the determination of the thermal expansion coefficient and thermal diffusivity, especially when preparing powdered

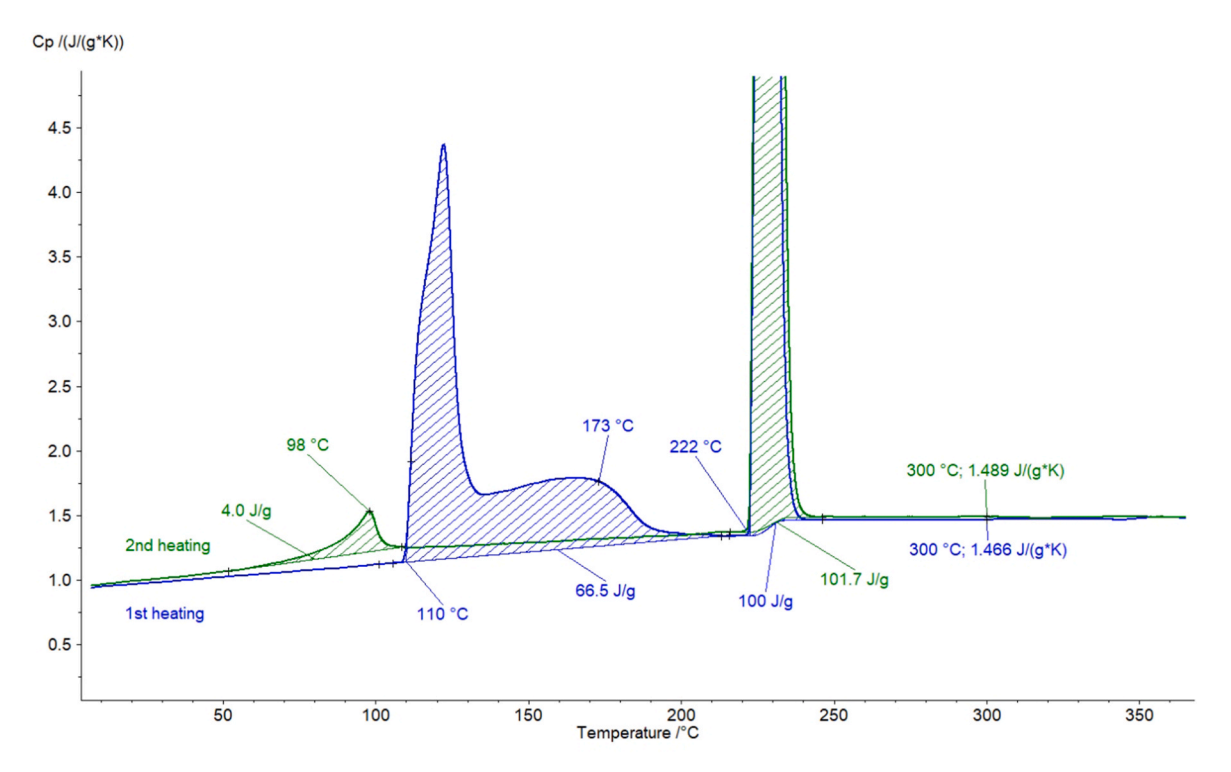


Fig. 4. Apparent specific heat capacity obtained by using the first and the second heating curves of the 50 mol % NaNO<sub>3</sub> - 50 mol % KNO<sub>3</sub> mixture.

samples. This is because the powder particle size and compaction can significantly affect the thermal conductivity and expansion behavior and can lead to inaccurate or inconsistent results. Proper sample preparation ensures homogeneity and reproducibility of the results. Fig. 5 shows the first heating and isothermal step at 210  $^{\circ}\text{C}$  for 24 h of two differently prepared samples. The significant difference in length change observed during the first heating step for both samples can be attributed to the sintering process occurring in the second sample. The second sample (pressed with 7 kN, 10 min) undergoes a sintering effect, where the length decreases by around 0.5 % during 24 h. However, for the first sample (pressed with 20 kN, 24 h) the length of the sample was almost stable for 24 h.

Fig. 6 shows the recalculated TMA results as the volume change through 3 heating cycles of the 50 mol % NaNO<sub>3</sub>-50 mol % KNO<sub>3</sub> mixture (first sample, pressed with 20 kN, 24 h) including solid and liquid phases. The TMA confirms the deductions made from the DSC measurements, where the first heating cycle shows a different behavior compared to subsequent heating cycles. The phase transition temperatures as well as the values of volume change in % are displayed in Fig. 6. To the best of our knowledge, no literature data are available for the thermal expansion of the solid phase in the 50 mol% NaNO<sub>3</sub> - 50 mol% KNO<sub>3</sub> mixture [27], which means, that these values have been obtained for the first time in the present paper.Density values of the liquid phase have been published and discussed in previous research papers [27, 31–34] and have been summarized in Ref. [27], where the average values are given as a polynomial:

$$\rho_{liquid} \big( g \, \big/ \, cm^3 \big) = - \, 6.891 \times 10^{-4} \cdot T(^{\circ}C) + 2.112$$

The obtained volume change values were recalculated to density using the reference value at 230  $^{\circ}$ C, equal to 1.953 g/cm<sup>3</sup>. A comparison of the recalculated liquid-phase density data from this work with average literature data, computed using the polynomial from Ref. [27], is provided in the supplementary material (Fig. 3s). The results show good agreement with previous values within a 0.15 % uncertainty range.

The information obtained from the thermal expansion of the 50 mol % NaNO $_3$  – 50 mol % KNO $_3$  mixture was used to determine thermal diffusivity by LFA analysis. The thickness of the sample plays an important role in determination of the thermal diffusivity according to

the equation [35]:

The LFA results are presented in Fig. 7 together with the DSC and TMA curves. The observed thermal effects and changes after the first and the second heating can be compared since all are related to the initial structural change of the sample.

An isoline plot of the *in-situ* heating from room temperature to 235  $^{\circ}$ C X-ray powder diffraction experiment of the first heating is shown in Fig. 8. X-ray diffraction signals of KNO<sub>3</sub> (*Pnma* symmetry) and NaNO<sub>3</sub> (*R*-3c symmetry) are clearly present. A phase transition is observed at ca. 110  $^{\circ}$ C, which is in good agreement with the DSC measurement. X-ray powder diffraction data provides insight into the phase transition of KNO<sub>3</sub> as it undergoes a change in symmetry from *Pnma* to *R*-3*m*.

Upon further heating above 110 °C two features become visible: firstly, the reflections of the high temperature KNO3 phase starts following a nonlinear progression and secondly, the intensity of the reflections associated with the NaNO<sub>3</sub> phase decreases, disappearing entirely above 185 °C. The concomitance of those 2 features suggest that sodium atoms are entering the high temperature structure of KNO<sub>3</sub> to exhibit a full solid solution (K,Na)NO<sub>3</sub> at elevated temperature. Above T  $\sim$ 180 °C, this solid solution is the only phase present, ultimately melting at T  $\sim$  220 °C. Above the melting temperature, the X-ray patterns clearly demonstrate the absence of any sharp peaks, displaying only broad humps, which are the typical signature of a liquid phase. While the data suggests the existence of a pure solid solution at high temperature, we note that this solid solution is not very homogenous in nature as illustrated by the noticeably broader reflections characterizing this phase. Additionally, X-ray powder diffraction allows us for a phase quantification by Rietveld as function of temperature which is presented in

As shown in Fig. 9, the decrease of the NaNO $_3$  phase is smooth until about 115 °C followed by a step and then a nearly linear decrease from about 130 °C until its complete disappearance. This behavior is consistent with the exsolution of sodium from the NaNO $_3$  phase to form a solid solution of (K,Na)NO $_3$ . The broad thermal event observed in the DSC measurement shown in Figs. 3 and 4 spanning the range from 130 to 190 °C is ascribed to the energy change required for the formation of the solid solution, confirmed by the non-ambient X-ray phase determination.

The sample was allowed to cool and crystallize (Fig. 10a). At first

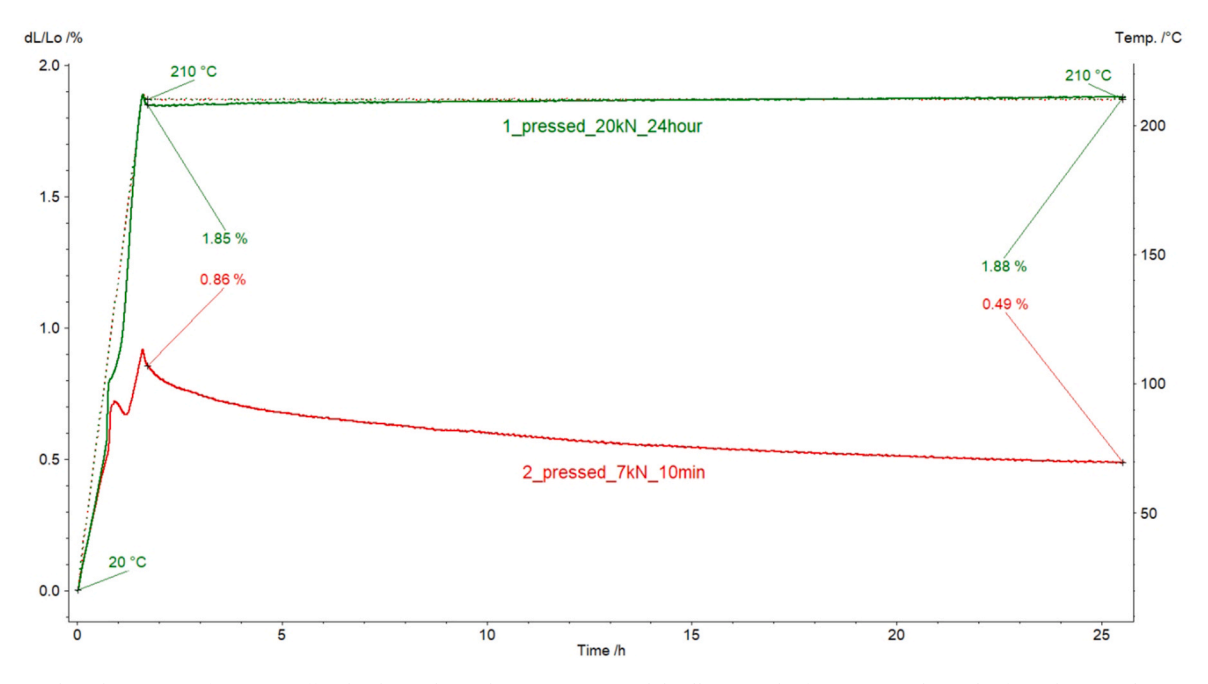


Fig. 5. TMA results: Observation of sintering effect by the isothermal step at 210 °C and dwell time 24 h of two prepared samples from the 50 mol % NaNO<sub>3</sub> - 50 mol % KNO<sub>3</sub> mixture. Dashed lines – temperature profile, solid lines – relative length change for two samples.

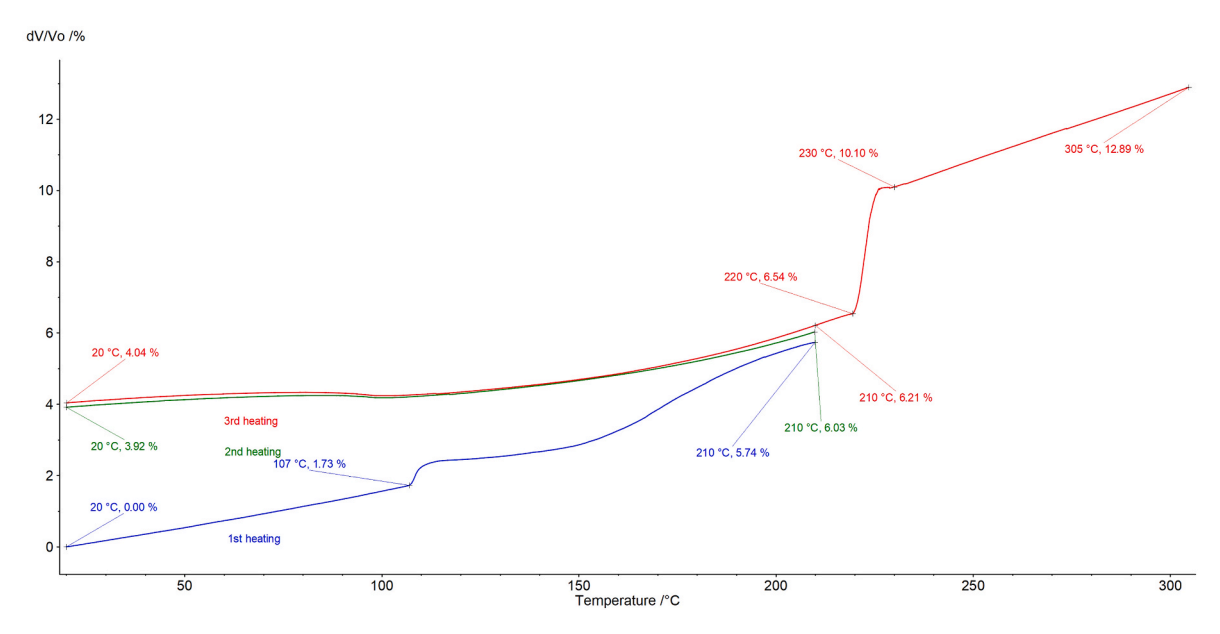


Fig. 6. TMA results: Temperature dependence of volume change through 3 heating cycles of the 50 mol % NaNO $_3$  - 50 mol % KNO $_3$  mixture including solid and liquid phases.

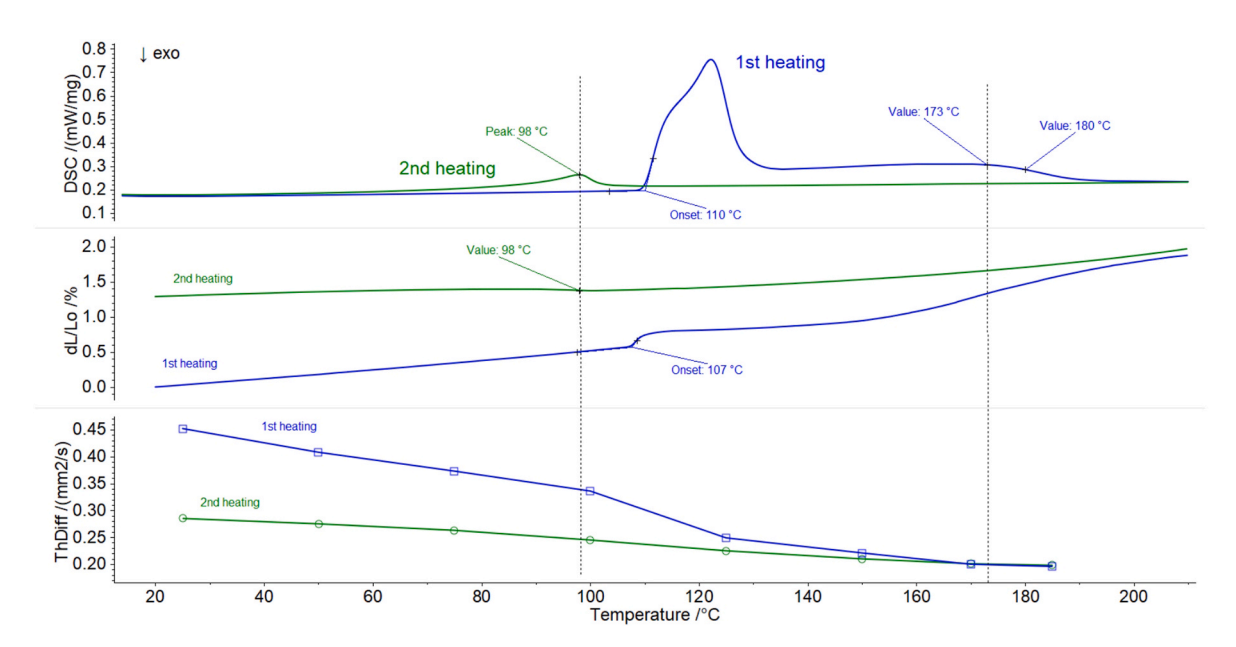


Fig. 7. Comparison of DSC, TMA, and LFA results for the first and the second heating of the 50 mol % NaNO<sub>3</sub>- 50 mol % KNO<sub>3</sub> mixture in the solid phase.

glance the data suggest the presence of only a single phase below temperatures of 220  $^{\circ}$ C; however, closer inspection reveals the presence of at least 2 phases with very similar cell parameters (Fig. 10b).

Upon cooling from 240  $^{\circ}$  C to 75  $^{\circ}$  C, the X-ray powder pattern is best described by a 2-phase model exhibiting the high temperature phase of KNO<sub>3</sub> (symmetry *R*-3*m*) with very similar cell parameters. This 2-phase model suggests that the X-ray powder diffraction supports the phase description shown in Fig. 1.

A structureless fit of the data (Pawley fit) is shown in Fig. 11. The corresponding cell parameters are a=5.2597(6) Å and c=9.2357(8) Å for phase 1 while phase 2 is characterized by a=5.2497(2) Å and c=9.2644(3) Å. By comparison, the cell dimensions obtained for the 1st heating are a=5.2562(7) Å and c=9.287(1) Å. While the length of the a-axis is comparable, the c-axis is significantly affected by the change in elemental composition as sodium is incorporated into the high temperature phase of KNO $_3$ . The two phases that are present in subsequent

heating cycles exhibit very similar cell parameters, which would suggest that their composition is also quite similar. Thus, although the presence of a pure NaNO<sub>3</sub> phase is not impossible at that stage (Fig. 1), the authors consider this possibility to be unlikely. This conjecture is further supported by the DSC data that shows a single melting event, implying that the chemical composition of both phases must be very similar to exhibit a single melting event within the resolution of our experiment.

The subsequent heating cycles were complemented by a second insitu X-ray diffraction heating study from 25  $^{\circ}$ C until 240  $^{\circ}$ C, although conducted with coarser temperature steps with data collected every 15  $^{\circ}$ C; see Fig. 12.

The data shown in Fig. 12 is in perfect agreement with the DSC data measured upon the 2nd heating: a transition around 95 °C followed by a melting around 220 °C. This confirms the existence of 3 phases: the first existing below about 95 °C, and the other two closely related *R-3m* phases that melt concomitantly. The results of the 2nd heating are in

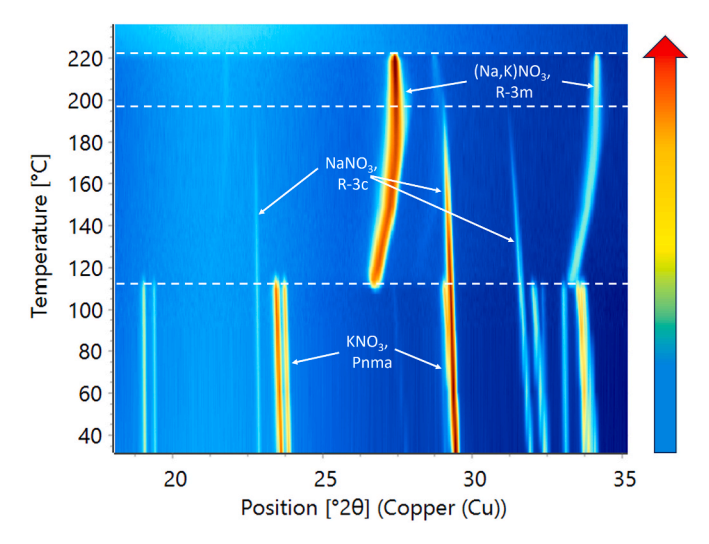


**Fig. 8.** Isoline plot of the *in-situ* heating X-ray powder diffraction experiment for the first heating (as indicated by the arrow) of a 50 mol % NaNO<sub>3</sub> - 50 mol % KNO<sub>3</sub> mixture.

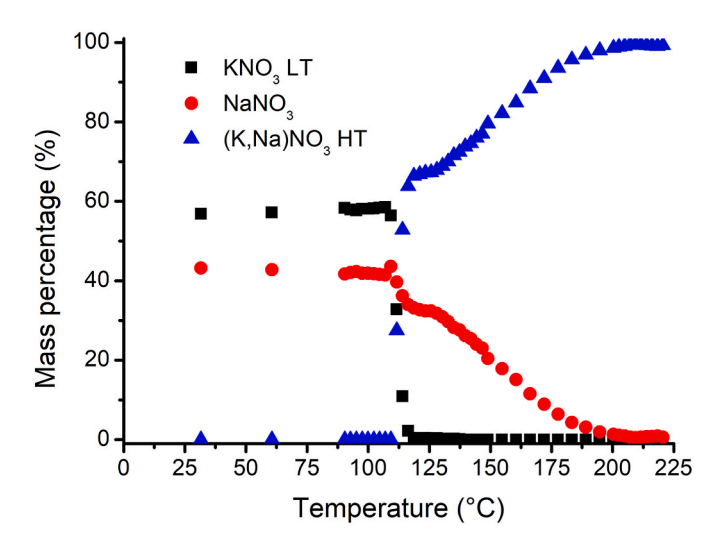


**Fig. 9.** Rietveld phase quantification results as function of temperature upon the first heating of a 50 mol %  $NaNO_3$ - 50 mol %  $KNO_3$  mixture. LT stands for the Low Temperature phase of  $KNO_3$  while HT stands for the High Temperature phase of the solid solution (K,Na) $NO_3$ .

closer agreement with the FTsalt phase diagram shown in Fig. 1, which consist from two solid solutions before melting  $ht-(K,[Na])NO_3 + ht-(Na,[K])NO_3$ .

## 4. Conclusions

In this work DSC, TMA, LFA, and non-ambient XRD were used for the study of the 50 mol % NaNO<sub>3</sub> - 50 mol % KNO<sub>3</sub> mixture. The experimental results obtained by DSC and TMA show significant differences between the first and the second heating of the prepared mixture, which is associated with a change in phase transition temperatures and in volume. This thermal behavior of the 50 mol % NaNO<sub>3</sub> – 50 mol % KNO<sub>3</sub> mixture also has an influence on the thermal diffusivity values. To explain this behavior in situ XRD measurements have been performed with two heating and cooling cycles. These data confirm the formation of metastable solid solution phases after the first heating and cooling. In addition, the XRD data also elucidate the phase transitions detected by the DSC and TMA measurements for the first heating cycle where the NaNO3 is continuously dissolving in the (Na,K)NO3 solid solution. The thermodynamic and thermophysical properties of the mixture are determined by thermal analysis. This data is supported by the X-ray diffractograms that provide the information about the phases that are present and their respective quantities.

We have shown that both the FTsalt as well as the FTfrtz phase diagrams (Figs. 1 and 2) [11–21] are required to explain the experimental results. The phase diagram from Fig. 2 is more related to the equilibrium state and from Fig. 1 representing metastable phases, which can be formed depending on the thermal and mechanical pretreatment of the sample. It was possible to prepare initially the stable phase of the 50 mol % NaNO<sub>3</sub> - 50 mol % KNO<sub>3</sub> mixture by using mechanical grinding process and keeping the sample for longer time in an exicator, which leads to complete separation of NaNO3 and KNO3 from the solid solution. However, within the framework of the performed experiments (DSC/TMA/LFA/XRD), it was not possible to observe the formation of the stable phase after the first heating and cooling cycle. Therefore the similar discrepancies have been observed for the experimental results from the previous studies [11–21]. Similar conclusions are presented in Ref. [36], where samples were annealed at least for 48 h at temperatures above 130 °C to achieve an equilibrium state of the solid solution phase, which aligns with the phase diagram presented in Fig. 2. Moreover in our work is shown, how the combination of thermal analysis DSC/TMA/LFA techniques with XRD analysis allows for a comprehensive characterization of salt samples.

# Declaration of competing interest

The authors declare that they have no known competing financial

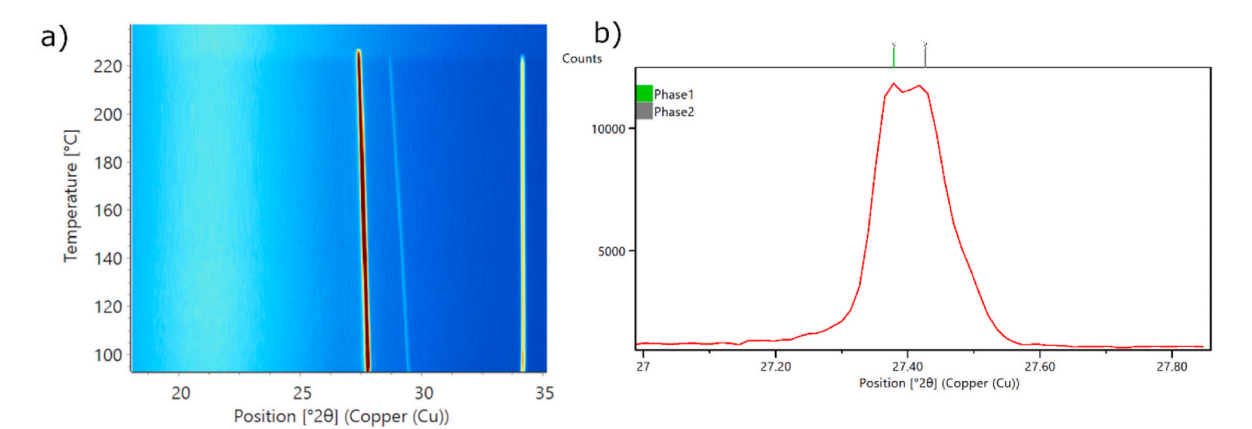


**Fig. 10.** a) Isoline plot of the in-situ X-ray powder diffraction experiment upon cooling from 240 °C to 95 °C of a 50 mol % NaNO<sub>3</sub> - 50 mol % KNO<sub>3</sub> mixture and b) zoom-in into the main reflection recorded at 180 °C.

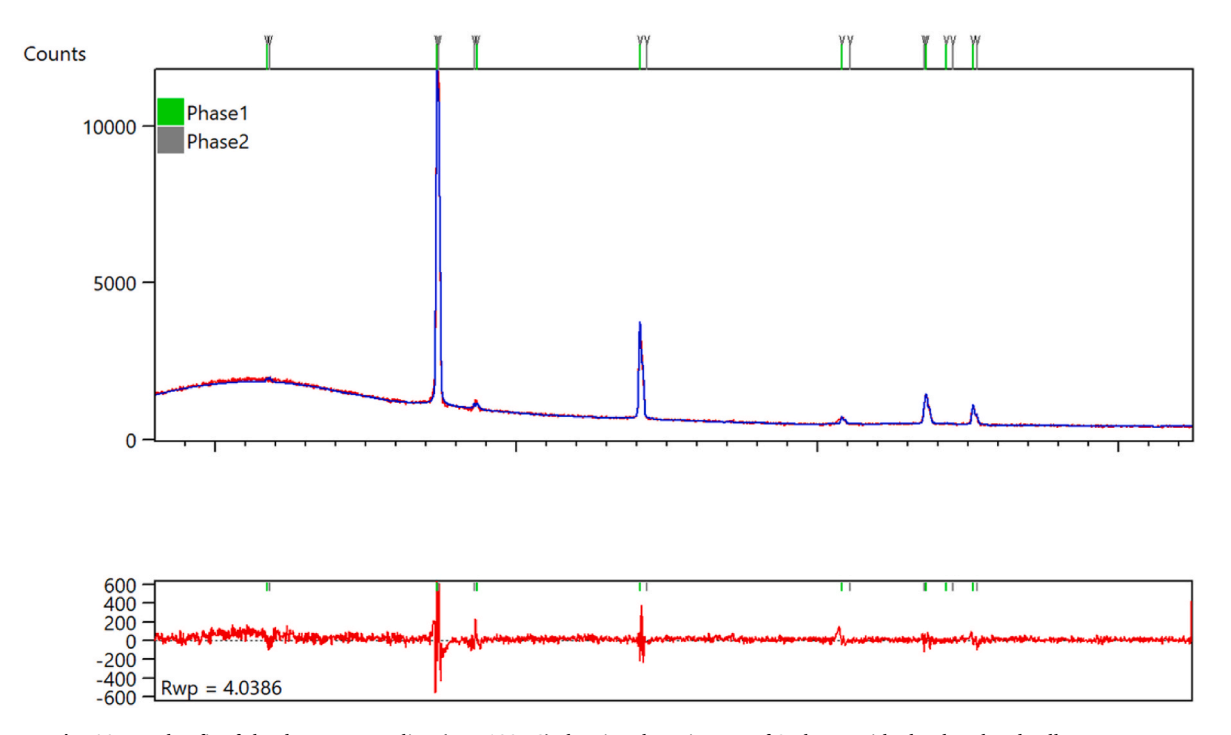


Fig. 11. Pawley fit of the data upon cooling (T = 188 °C) showing the existence of 2 phases with closely related cell parameters.

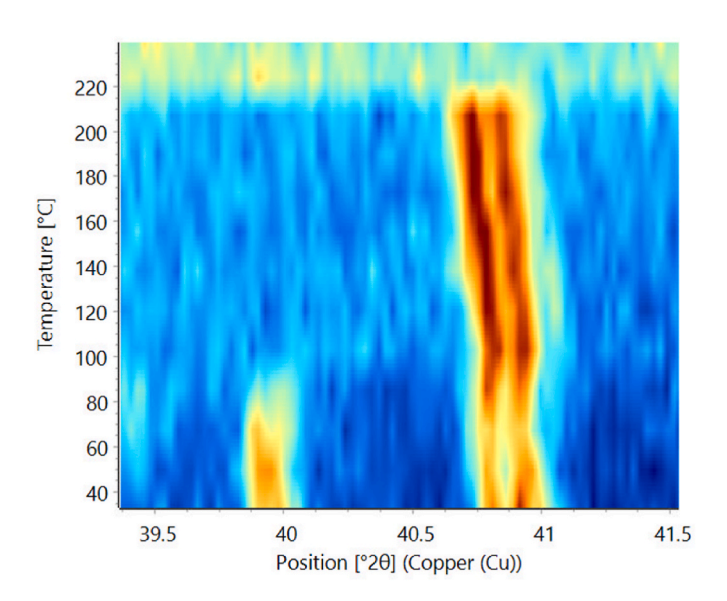


Fig. 12. Isoline plot of the in-situ X-ray powder diffraction experiment of the 2nd heating from 25  $^{\circ}C$  to 240  $^{\circ}C$  of a 50 mol % NaNO $_3$  - 50 mol % KNO $_3$  mixture.

interests or personal relationships that could have appeared to influence the work reported in this paper.

# Acknowledgements

Part of this work was done in the framework of the PCM-Screening-2 project, which is supported by the Federal Ministry of Economic Affairs and Climate Action, Germany (FKZ 03EN6005D). We would like to express our gratitude to Dr. Jan Hanss (NETZSCH A&T) and to Prof. Hans Jürgen Seifert (KIT, IAM-AWP) for their invaluable assistance, guidance, and insightful discussions throughout this work.

During the preparation of this work, the authors used ChatGPT-40 by OpenAI in order to assist with language editing and text improvement. After using this tool, the authors reviewed and edited the content as needed and take full responsibility for the content of the publication.

## Appendix A. Supplementary data

Supplementary data to this article can be found online at https://doi.org/10.1016/j.jmrt.2025.03.128.

## References

- Bonk A, Braun M, Sötz VA, Bauer T. Solar Salt pushing an old material for energy storage to a new limit. Appl Energy 2020;262:114535.
- [2] Steinbrecher J, Hanke A, Braun M, Bauer T, Bonk A. Stabilization of solar salt at 650 °C – thermodynamics and practical implications for thermal energy storage systems. Sol Energy Mater Sol Cell 2023;258:112411.
- [3] Svobodova-Sedlackova A, Palacios A, Jiang Z, Fernández Renna AI, Ding Y, Navarro H, Barreneche C. Thermal stability and durability of solar salt-based nanofluids in concentrated solar power thermal energy storage: an approach from the effect of diverse metal alloys corrosion. J Energy Storage 2024;75:109715.
- [4] Villada C, Bonk A, Bauer T, Bolívar F. High-temperature stability of nitrate/nitrite molten salt mixtures under different atmospheres. Appl Energy 2018;226:107–15.
- [5] Olivares RI. The thermal stability of molten nitrite/nitrate salt for solar thermal energy storage in different atmospheres. Sol Energy 2012;86(9):2576–83.
- [6] Wu Y-T, Li Y, Ren N, Ma C-F. Improving the thermal properties of NaNO<sub>3</sub>-KNO<sub>3</sub> for concentrating solar power by adding additives. Sol Energy Mater Sol Cell 2017; 160:263–8.
- [7] Janz GJ, Allen CB, Bansal N, Murphy R, Tomkins R. Physical properties data compilations relevant to energy storage.II. Molten salts: data on single and multicomponent salt systems.National Standard Reference Data System; NSRDS-NBS 61, Part II. US Department of Commerce, National Bureau of Standards; 1979. p. 396–411.
- [8] Delise T, Tizzoni AC, Ferrara M, Corsaro N, D'Ottavi C, Giaconia A, Turchetti L, Annesini MC, Telling M, Sau S, Licoccia S. New solid phase of KNO<sub>3</sub> – NaNO<sub>3</sub> salt mixtures studied by neutron scattering and differential scanning calorimetry analysis. AIP Conf Proc 2018;2033(1):080001.
- [9] Nunes VMB, Queirós CS, Lourenço MJV, Santos FJV, Nieto de Castro CA. Molten salts as engineering fluids – a review: Part I. Molten alkali nitrates. Appl Energy 2016;183:603–11.
- [10] Berg RW, Kerridge DH. The NaNO<sub>3</sub>/KNO<sub>3</sub> system: the position of the solidus and sub-solidus. Dalton Trans 2004;1:2224–9.
- [11] Sergeev D, et al. Phase equilibria in the reciprocal NaCl–KCl–NaNO<sub>3</sub>–KNO<sub>3</sub> system. Calphad 2015;51:111–24.
- [12] Bale CW, Chartrand P, Degterov SA, Eriksson G, Hack K, Ben Mahfoud R, Melançon J, Pelton AD, Petersen S. FactSage thermochemical software and databases. Calphad 2002;26:189–228.
- [13] Beneš O, et al. A DSC study of the NaNO<sub>3</sub>-KNO<sub>3</sub> system using an innovative encapsulation technique. Thermochim Acta 2010;509(Issue 1–2):62–6.

- [14] Zhang X, Tian J, Xu K, Gao Y. Thermodynamic evaluation of phase equilibria in NaNO<sub>3</sub>-KNO<sub>3</sub> system. J Phase Equil 2003;24:441–6.
- [15] Dessureault Y, Sangster JM, Pelton AD. Critical evaluation of thermodynamic data and phase diagrams of the systems AOH-AX, ANO<sub>3</sub>-AX, ANO<sub>3</sub>-BNO<sub>3</sub>, AOH-BOH where A, B=Li, Na, K and X=Cl, F, NO<sub>3</sub>, OH. J. Chim. Phys. 1990;87:407–53.
- [16] Jriri T, Rogez J, Mathieu JC, Ansara I. Thermodynamic analysis of the CsNO<sub>3</sub>-KNO<sub>3</sub>-NaNO<sub>3</sub> system. J Phase Equil 1999;20:515–25.
- [17] Robelin C, Chartrand P, Pelton AD. Thermodynamic evaluation and optimization of the (NaNO<sub>3</sub>-KNO<sub>3</sub>-Na<sub>2</sub>SO<sub>4</sub>-K<sub>2</sub>SO<sub>4</sub>) system. J Chem Thermodyn 2015;83:12–26.
- [18] Xu K, Chen Y. Temperature-dependent Raman spectra of mixed crystals of NaNO3-KNO3: evidence for limited solid solutions. J Raman Spectrosc 1999;30: 173-9.
- [19] Xu K, Chen Y. Raman spectroscopic studies of mixed crystals of NaNO3–KNO3 quenched from different temperatures: evidence for limited solid solutions in the system. J Raman Spectrosc 1999;30:441–8.
- [20] Greis O, Bahamdan KM, Uwais BM. The phase diagram of the system NaNO<sub>3</sub>-KNO<sub>3</sub> studied by differential scanning calorimetry. Thermochim Acta 1985;86:343–50.
- [21] Zamali H, Jemal M. Diagrammes de phases des systemes binaires KNO<sub>3</sub>-CsNO<sub>3</sub> et KNO<sub>3</sub>-NaNO<sub>3</sub>. J Therm Anal 1994;41:1091–9.
- [22] Wang YB, Ryan DH, Altounian Z. Structural and thermal studies of nitrate glasses. J Non-Cryst Solids 1996;205–207:221–4.
- [23] Sergeev D, Simanjuntak EK, Ziegner M, Müller M. Thermodynamic properties of KCaCl(NO<sub>3</sub>)<sub>2</sub> compound and influence of kinetic effects. Calphad 2023;80:102519.
- [24] Degen T, Sadki M, Bron E, König U, Nénert G. The HighScore suite. Powder Diffr 2014;29(S2):S13–8. https://doi.org/10.1017/S0885715614000840.
- [25] Grosu Y, González-Fernández L, Nithiyanantham U, Faik A. Wettability control for correct thermophysical properties determination of molten salts and their nanofluids. Energies 2019;12:3765.

- [26] Zhao Q-G, Hu C-X, Liu S-J, Guo H, Wu Y-T. The thermal conductivity of molten NaNO<sub>3</sub>, KNO<sub>3</sub>, and their mixtures. Energy Proc 2017;143:774–9.
- [27] Bauer T, Laing D, Tamme R. Overview of PCMs for concentrated solar power in the temperature range 200 to 350°C. AST 2010;74:272–7.
- [28] Yang H, Gallagher R, Chartrand P, Gheribi AE. Development of a molten salt thermal conductivity model and database for advanced energy systems. Sol Energy 2023;256:158–78.
- [29] Kamimoto M. Thermodynamic properties of 50 mole% NaNO<sub>3</sub>-50% KNO<sub>3</sub> (HTS2). Thermochim Acta 1981;49:319-31.
- [30] Rogers DJ, Janz GJ. Melting-crystallization and premelting properties of sodium nitrate-potassium nitrate: enthalpies and heat capacities. J Chem Eng Data 1982; 27-424-8
- [31] Nissen DA. Thermophysical properties of the equimolar mixture sodium nitratepotassium nitrate from 300 to 600°C. J Chem Eng Data 1982;27:269–73.
- [32] Carling RW, et al. Molten nitrate salt technology development" Sandia Laboratory Report, SAND80-8052; 1981.
- [33] Schinke H, Sauerwald F. Density measurements: on the volume change during melting and the melting process of inorganic salts. Z Anorg Allg Chem 1960;304: 25–36 (in German).
- [34] Murgulescu IG, Zuca S. Viscosity of binary mixtures of molten nitrates as a function of ionic radius—II. Electrochim Acta 1969;14:519–26.
- [35] Parker WJ, Jenkins RJ, Butler CP, Abbott GL. Flash method of determining thermal diffusivity, heat capacity, and thermal conductivity. J Appl Phys 1961;32(9): 1679–84.
- [36] Benages-Vilau R, Calvet T, Cuevas-Diarte MA, Oonk HAJ. The NaNO<sub>3</sub>–KNO<sub>3</sub> phase diagram. Phase Transitions 2015;89(1):1–20.